J|A|C|S ARTICLES

Published on Web 06/15/2010

The Role of Order, Nanocrystal Size, and Capping Ligands in the Collective Mechanical Response of Three-Dimensional Nanocrystal Solids

Paul Podsiadlo,*,† Galyna Krylova,† Byeongdu Lee,‡ Kevin Critchley,§ David J. Gosztola,† Dmitri V. Talapin,†,|| Paul D. Ashby,⊥ and Elena V. Shevchenko*,†

Center for Nanoscale Materials, Argonne National Laboratory, Argonne, Illinois 60439, Advanced Photon Source, Argonne National Laboratory, Argonne, Illinois 60439, School of Physics, University of Leeds, Leeds, LS29JT, United Kingdom, Chemistry Department, University of Chicago, Chicago, Illinois 60637, and The Molecular Foundry, Lawrence Berkeley National Laboratory, Berkeley, California 94720

Received January 18, 2010; E-mail: eshevchenko@anl.gov; ppodsiadlo@anl.gov

Abstract: Chemically synthesized PbS, CdSe, and $CoPt_3$ nanocrystals (NCs) were self-assembled into highly periodic supercrystals. Using the combination of small-angle X-ray scattering, X-ray photoelectron spectroscopy, infrared spectroscopy, thermogravimetric analysis, and nanoindentation, we correlated the mechanical properties of the supercrystals with the NC size, capping ligands, and degree of ordering. We found that such structures have elastic moduli and hardnesses in the range of ~0.2−6 GPa and 10−450 MPa, respectively, which are analogous to strong polymers. The high degree of ordering characteristic to supercrystals was found to lead to more than 2-fold increase in hardnesses and elastic moduli due to tighter packing of the NCs, and smaller interparticle distance. The nature of surface ligands also significantly affects the mechanical properties of NCs solids. The experiments with series of 4.7, 7.1, and 13 nm PbS NCs revealed a direct relationship between the core size and hardness/modulus, analogous to the nanoparticle-filled polymer composites. This observation suggests that the matrices of organic ligands have properties similar to polymers. The effective moduli of the ligand matrices were calculated to be in the range of ~0.1−0.7 GPa.

Introduction

Colloidal nanocrystal (NC) solids has been a subject of intense research in the past two decades.[1] Quantum size effect, plasmon resonance, and superparamagnetism discovered at nanoscale attracted a great attention of the researchers because of a great promise of such properties for a wide range of applications including electronic, magnetic, and optical devices.[2] Some notable examples of recent developments include field-effect transistors,[3−5] light-emitting devices,[6] photodetectors,[7] photoconductors,[8] and solar cells.[9]

The development of efficient synthetic methods for preparation of highly monodisperse NCs that can serve as artificial atoms allows obtaining highly periodic two- (2D) and three-dimensional (3D) structures[10,11] such as NC-films and 3D faceted supercrystals (SCs).[11] The availability of a large variety of NC compositions and properties and proper control over particle−particle interactions allows obtaining mono-,[11] binary- (two types of NCs),[12−14] ternary (three types of NCs) periodic superstuctures,[15,16] or even dodecagonal quasicrystals consisting of two different types of NCs.[17] In comparison to NC films,

† Center for Nanoscale Materials, Argonne National Laboratory.
‡ Advanced Photon Source, Argonne National Laboratory.
§ University of Leeds.
|| University of Chicago.
⊥ Lawrence Berkeley National Laboratory.

(1) Alivisatos, A. P. *Science* **1996**, *271*, 933–937.
(2) Talapin, D. V.; Lee, J.-S.; Kovalenko, M. V.; Shevchenko, E. V. *Chem. Rev.* **2009**, *110*, 389–458.
(3) Talapin, D. V.; Murray, C. B. *Science* **2005**, *310*, 86–89.
(4) Kovalenko, M. V.; Scheele, M.; Talapin, D. V. *Science* **2009**, *324*, 1417–1420.
(5) Yu, D.; Wang, C. J.; Guyot-Sionnest, P. *Science* **2003**, *300*, 1277–1280.
(6) Caruge, J. M.; Halpert, J. E.; Wood, V.; Bulovic, V.; Bawendi, M. G. *Nat. Photonics* **2008**, *2*, 247–250.
(7) Konstantatos, G.; Howard, I.; Fischer, A.; Hoogland, S.; Clifford, J.; Klem, E.; Levina, L.; Sargent, E. H. *Nature* **2006**, *442*, 180–183.
(8) Nakanishi, H.; Bishop, K. J. M.; Kowalczyk, B.; Nitzan, A.; Weiss, E. A.; Tretiakov, K. V.; Apodaca, M. M.; Klajn, R.; Stoddart, J. F.; Grzybowski, B. A. *Nature* **2009**, *460*, 371–375.
(9) Gur, I.; Fromer, N. A.; Geier, M. L.; Alivisatos, A. P. *Science* **2005**, *310*, 462–465.
(10) Murray, C. B.; Kagan, C. R.; Bawendi, M. G. *Ann. Rev. Mater. Sci.* **2000**, *30*, 545–610.
(11) Murray, C. B.; Kagan, C. R.; Bawendi, M. G. *Science* **1995**, *270*, 1335–1338.
(12) Redl, F. X.; Cho, K. S.; Murray, C. B.; O'Brien, S. *Nature* **2003**, *423*, 968–971.
(13) Shevchenko, E. V.; Talapin, D. V.; Kotov, N. A.; O'Brien, S.; Murray, C. B. *Nature* **2006**, *439*, 55–59.
(14) Kalsin, A. M.; Fialkowski, M.; Paszewski, M.; Smoukov, S. K.; Bishop, K. J. M.; Grzybowski, B. A. *Science* **2006**, *312*, 420–424.
(15) Shevchenko, E. V.; Kortright, J. B.; Talapin, D. V.; Aloni, S.; Alivisatos, A. P. *Adv. Mater.* **2007**, *19*, 4183–4188.
(16) Evers, W. H.; Friedrich, H.; Filion, L.; Dijkstra, M.; Vanmaekelbergh, D. *Angew. Chem., Int. Ed.* **2009**, *48*, 9655–9657.

SCs usually have a higher degree of ordering as evidenced by larger size of crystalline domains.[18] Besides their aesthetic appeal, the precise ordering offers a unique opportunity to control the electronic coupling between the individual NCs which can lead to new collective properties such as vibrational coherence,[19] reversible metal-to-insulator transitions,[20] enhanced p-type conductivity,[21] spin-dependent electron transport,[22] enhanced ferro- and ferrimagnetism,[23,24] and variable range electron hoping,[25] in 2D and 3D superstructures.

To date, very little is known about the mechanical properties of NC solids. The progress in this field is limited by reports on mechanical properties of randomly organized electrophoretically deposited CdSe NC films,[26−28] 3D structures assembled from 150-nm gold supraspheres[6] and 2D periodic free-standing film,[29] that revealed polymer-like behavior with moduli as high as 10 GPa for the thick NCs films and ∼6 GPa for free-standing monolayers of Au NCs.[29] On the other hand, molecular dynamics (MD) simulations have predicted a significantly smaller Young's modulus. Thus, Young's modulus of ∼1 GPa was simulated for 3D assemblies of 1.7 nm Au NCs stabilized with dodecanethiol.[30] However, to the best of our knowledge, the mechanical properties of SCs self-assembled from NCs have not been studied and many questions such as the effect of degree of ordering, size of NCs, type of capping ligands, and so forth are still unanswered. The diverse field of applications of NC solids requires the understanding of their mechanical properties, as a criterion for device robustness and durability. NC solids with different degree of ordering are an excellent platform to study the role of structural organization in the collective mechanical response of the system. The wide size and compositional range of NCs as well as diversity of the capping ligands at their surface provide a great opportunity to perform a systematic study of the mechanical properties of NC solids self-assembled from different types of NCs.

Our study is aimed at the understanding of the role of the size of NCs, degree of nanocrystal ordering, chemical composition of nanocrystals, and the nature of capping ligands in the collective mechanical response of NC solids. We used the nanoindentation technique to probe the mechanical properties of both highly ordered single-component SCs and drop-casted films with lower degree of ordering.[18] Nearly spherical PbS, CdSe, and $CoPt_3$ NCs with different sizes and capping ligands were chosen as model systems.

Experimental Procedures

Materials. Toluene, isopropyl alcohol (*i*-PrOH), diphenyl ether, ethanol, *n*-hexane, 1-octadecene (ODE), oleic acid (OA), trioctylphosphine oxide (TOPO), hexadecylamine (HDA), dodecanoic acid (DDA), pyridine (PY), bis(trimethylsilyl)sulfide ($(TMS)_2S$), and 1-adamantanecarboxylic acid (ACA) were all purchased from Sigma-Aldrich. The chemicals were at least of ACS purity. Trioctylphosphine (TOP) and 1,2-hexadecandiol were obtained from Fluka. $PbAc_2 \cdot 3H_2O$ and 1,2-dichlorobenzene were purchased from Acros Chemicals. Cobalt carbonyl ($Co_2(CO)_8$, stabilized with 1−5% hexane), and platinum(II)-acetylacetonate ($Pt(acac)_2$, 98%) were obtained from Strem. Glass/ITO coverslips (2.5 cm ×2.5 cm, 0.5 mm thick) used for growing the SCs were obtained from Delta Technologies (Stilwater, MN). The coverslips were diced into 4 mm wide strips with a wafer dicing saw. Glass test tubes (0.8 cm i.d. by 10 cm long) used for SCs growth were obtained from Fisher Scientific.

Nanocrystals Synthesis. CdSe nanocrystals (4.6 nm diameter) were synthesized according to the protocol described in ref 31. The PbS NCs were synthesized according to the method of Hines and Scholes.[32] The standard procedure gave ∼7.1 nm PbS NCs. Thirteen-nanometers PbS NCs were formed by reducing the ODE volume from 10 to 6 mL. The 4.7 nm PbS NCs were achieved by reducing the OA volume from 20 to 15 mL and increasing the volume of ODE to 15 mL. The 6.5 and 10 nm $CoPt_3$ NCs were prepared following the procedure described in ref 33. The sizes of the NCs used in this work were determined using grazing-incidence small-angle X-ray scattering (GISAXS) and high-resolution transmission electron microscopy (HRTEM) measurements. The standard deviations of all NCs samples were ∼5% as determined from GISAXS measurements. Samples for TEM characterization were prepared by placing 1−2 μL of a diluted (0.1 mg/mL) solution in toluene on a carbon-coated copper grid (Ted-Pella). The excess solvent was removed after 10 s with a filter paper. Dynamic light scattering measurements performed using the ZetaSizer (Malvern Instruments) revealed closely matching size distributions of the NCs in the solution, that is, CdSe = 5.24 ± 0.67 nm, $PbS_{4.7}$ = 5.39 ± 0.83 nm, $PbS_{7.1}$ = 7.42 ± 0.96 nm, PbS_{13} = 13.94 ± 2.77 nm.

Preparation of Nanocrystal Solids. The SCs were prepared on glass coverslips coated with a transparent conductive layer of indium tin oxide (ITO) by the method of slow destabilization of NCs with a nonsolvent.[34] The transparent conductive substrates were necessary for positioning of the indenter head and imaging of the SCs in a SEM. In a typical preparation, a single glass/ITO strip was placed vertically in a vertically positioned glass test tube and 0.5 mL of toluene solution of NCs (∼1×10^{12} NCs/mL) was added to the bottom of the tube. Subsequently, 0.8 mL of *i*-PrOH was gently added on top of the NC solution avoiding the disturbance and intermixing of the two solutions. The tubes were then sealed with Parafilm and allowed to sit undisturbed for a week (growth of SCs from smaller NCs can take as long as 3 weeks). Upon complete diffusional intermixing of the solvents, the solutions were carefully withdrawn with Pasteur pipettes and discarded. The substrates were removed, air-dried, and stored for subsequent characterization. For SCs with new ligand additions, the concentration of original ligands on NCs was calculated by weighing dry films of NCs and

(17) Talapin, D. V.; Shevchenko, E. V.; Bodnarchuk, M. I.; Ye, X. C.; Chen, J.; Murray, C. B. *Nature* **2009**, *461*, 964–967.
(18) Lee, B.; Podsiadlo, P.; Rupich, S.; Talapin, D. V.; Rajh, T.; Shevchenko, E. V. *J. Am. Chem. Soc.* **2009**, *131*, 16386–16389.
(19) Courty, A.; Mermet, A.; Albouy, P. A.; Duval, E.; Pileni, M. P. *Nat. Mater.* **2005**, *4*, 395–398.
(20) Collier, C. P.; Saykally, R. J.; Shiang, J. J.; Henrichs, S. E.; Heath, J. R. *Science* **1997**, *277*, 1978–1981.
(21) Urban, J. J.; Talapin, D. V.; Shevchenko, E. V.; Kagan, C. R.; Murray, C. B. *Nat. Mater.* **2007**, *6*, 115–121.
(22) Black, C. T.; Murray, C. B.; Sandstrom, R. L.; Sun, S. H. *Science* **2000**, *290*, 1131–1134.
(23) Sun, S. H.; Murray, C. B.; Weller, D.; Folks, L.; Moser, A. *Science* **2000**, *287*, 1989–1992.
(24) Cheon, J.; Park, J. I.; Choi, J. S.; Jun, Y. W.; Kim, S.; Kim, M. G.; Kim, Y. M.; Kim, Y. J. *Proc. Nat. Acad. Sci. U.S.A.* **2006**, *103*, 3023–3027.
(25) Tran, T. B.; Beloborodov, I. S.; Lin, X. M.; Bigioni, T. P.; Vinokur, V. M.; Jaeger, H. M. *Phys. Rev. Lett.* **2005**, *95*, 076806.
(26) Klajn, R.; Bishop, K. J. M.; Fialkowski, M.; Paszewski, M.; Campbell, C. J.; Gray, T. P.; Grzybowski, B. A. *Science* **2007**, *316*, 261–264.
(27) Banerjee, S.; Jia, S. G.; Kim, D. I.; Robinson, R. D.; Kysar, J. W.; Bevk, J.; Herman, I. P. *Nano Lett.* **2006**, *6*, 175–180.
(28) Lee, D.; Jia, S. G.; Banerjee, S.; Bevk, J.; Herman, I. P.; Kysar, J. W. *Phys. Rev. Lett.* **2007**, *98*, 026103.
(29) Mueggenburg, K. E.; Lin, X. M.; Goldsmith, R. H.; Jaeger, H. M. *Nat. Mater.* **2007**, *6*, 656–660.
(30) Landman, U.; Luedtke, W. D. In *Nanoparticle Assemblies Meeting*; Royal Soc. Chemistry: Liverpool, England, 2003; pp 1−22.
(31) Talapin, D. V.; Rogach, A. L.; Kornowski, A.; Haase, M.; Weller, H. *Nano Lett.* **2001**, *1*, 207–211.
(32) Hines, M. A.; Scholes, G. D. *Adv. Mater.* **2003**, *15*, 1844–1849.
(33) Shevchenko, E. V.; Talapin, D. V.; Rogach, A. L.; Kornowski, A.; Haase, M.; Weller, H. *J. Am. Chem. Soc.* **2002**, *124*, 11480–11485.
(34) Talapin, D. V.; Shevchenko, E. V.; Kornowski, A.; Gaponik, N.; Haase, M.; Rogach, A. L.; Weller, H. *Adv. Mater.* **2001**, *13*, 1868–1871.

calculating amount of the organic component based on thermogravimetric analysis (Table S1). With this information, a 6-fold excess of a new ligand was added to the NCs solution before addition of the *i*-PrOH layer. The films of the NCs were obtained by air-drying droplets of the same dispersions used in assembly of SCs, at room temperature, on the ITO substrates. Several-micrometers-thick regions of the drop-casted solid (either edges or centers of residual stains remaining after evaporation of solvent) were chosen for characterization with nanoindentation. The thickness of the SCs was comparable with the thickness of films.

Characterization Methods. Low-resolution electron microscopy images were obtained with a JEOL 7500 Scanning Electron Microscope (SEM) equipped with a transmission electron detector. The images were acquired at 30 kV accelerating voltage with samples deposited on standard Cu grids. TEM and HRTEM images were obtained using a FEI Tecnai F30 field emission analytical transmission electron microscope operating at an acceleration voltage of 300 kV. High-resolution SEM images were obtained with an FIB FEI Nova 600 NanoLab SEM operated at 18 kV accelerating voltage. Optical images were obtained with a Zeiss Axio Imager microscope. Thermogravimetric (TGA) measurements were performed with a Mettler-Toledo STAR^e TGA/SDTA851^e system operated under an inert, N_2 atmosphere. TGA samples of NCs films were prepared by evaporating concentrated NCs solutions inside Al crucibles, followed by drying under vacuum at room temperature. SC samples were first extracted from their test tubes using toluene and sonication, followed by evaporation in the Al crucibles. XPS spectra were obtained using a Thermo Electron Corporation ESCA Lab 250 with a chamber pressure maintained below 5×10^{-9} mbar during acquisition. A monochromated Al K alpha X-ray source (15 kV; 150 W) irradiated the samples, with a spot diameter of approximately 0.5 mm. The spectrometer was operated in Large Area XL magnetic lens mode using a pass energy of 150 and 20 eV for survey and detailed scans, respectively. The spectra were obtained with a takeoff angle of 90°. High-resolution spectra were fitted using Avantage (Thermo VG software package) peak fitting algorithms. All spectra have been normalized to the C 1s peak (284.6 eV). Samples were prepared by drying the NCs dispersion on a freshly cleaned gold coated substrate ($\sim$1 cm^2); in some cases, the thickness of the NCs layer was sufficient to attenuate the gold signal entirely. Fourier transform infrared (FTIR) measurements were conducted using a Bruker, Vertex 70 spectrometer. Dried samples in the amount of $\sim$100 μg were characterized by placing directly on the top of the ATR crystal. Raman spectra were measured on a Raman microscope (Renishaw, inVia) with excitation wavelengths of 514 and 613 nm and a spot size of $\sim$1 μm. All spectra were measured using a 100$\times$ microscope objective to focus the laser excitation (5 mW) onto the samples as well as collect the scattered light. GISAXS data were acquired at the Argonne National Laboratory's Advanced Photon Source. Sample to detector distance was $\sim$2 m, and two X-ray energies of 8 and 12 keV were used for varying the resolution of diffractogram.

Nanoindentation Measurements. The experiments were conducted with an Asylum Research, MFP-3D Atomic Force Microscope with a low force nanoindentation accessory and Berkovich tip under either load or displacement control. The loading/unloading time was chosen at 6 s each, with a holding time of 8 s applied at the maximum load allowing creep at the beginning of the unloading phase to be less than 1 nm/s (near the drift rate of the instrument). The creep was established from successive experiments. The maximum load range for each sample was chosen such that the penetration depth did not exceed the 10−20% of sample's thickness to avoid influence of the substrate on the measured data (under the load control). The thickness of the samples was large enough that 10−20% range of indentation depth did not show the increase in mechanical properties which otherwise would indicate the existence of the substrate effect.[35] The indentation load was typically applied in increments of 50 μN, with the largest load of 600 μN applied for the largest SCs composed of 4.7 nm PbS NCs. Thus, the 600 μN load for large SCs from 4.7 nm PbS NCs corresponded to at most 1.4 μm, which is significantly smaller than thickness of SCs. For large SCs, given their large surface area, multiple indentations were performed on the same SC. In all cases, at least 3 randomly picked SCs with flat top surface were tested for each sample type. Similarly, for statistical comparisons, the same number of measurements was performed on the films of the NCs with at least 3 randomly chosen thick areas of the sample. The surface roughness of the samples (both films and SCs) was not considered since the indentation depth was greater than the thickness variation across the samples. The indentation modulus and hardness were determined from the load−displacement curves by applying the Oliver and Pharr analysis.[36]

Results and Discussion

With the goal of better understanding the mechanical properties of the SCs, we synthesized a series of PbS NCs samples with varying core sizes (4.7, 7.1, and 13 nm), all stabilized with oleic acid (OA) (Figures S1 and S2). For comparison, we also synthesized 4.6 nm CdSe NCs, which have a different composition of inorganic core and surface ligands: that is, trioctylphosphine oxide (TOPO), trioctylphosphine (TOP), and hexadecylamine (HDA); and $CoPt_3$ NCs stabilized by a mixture of 1-hexadecylamine (HDA) and 1-adamantane carboxylic acid (ACA) (Figures S1 and S2). Characterization of the SCs with optical and electron microscopes revealed a high density of faceted crystallites, at least several micrometers in size (Figure 1 and Figure S3). The flat SCs shown in Figure 1 were the typical samples tested with nanoindentation, although as can be seen in Figure S3, the SCs can adopt many shapes, just as in traditional atomic and molecular crystals. We found that the smallest CdSe and PbS NCs formed the largest SCs (as large as 200 μm for PbS and nearly 100 μm for CdSe), and the size of the crystallites decreased with increasing NCs sizes, which is probably associated with higher surface ligands-to-NC core ratio in the case of smaller NCs and hence with slower destabilization of their colloidal solutions. In fact, the assembly of the 4.7 nm NCs could take as long as 3 weeks to complete, while the SCs from 13 nm NCs could be finished in as little as 3−4 days. This observation is also in agreement with previously published results confirming the lower probability of twinning due to dominant ligand−ligand interactions and higher twinning energy in the systems with smaller NCs.[37] High-resolution SEM (Figure 1) revealed tightly packed surfaces of the NCs. High degree of ordering of NCs in 3D superstructures was also confirmed with GISAXS experiments. (Figure S4 and Table S2) The GISAXS measurements revealed primarily face-centered cubic (fcc) organization, although body-centered cubic (bcc) and hexagonal close-packed (hcp) structures were also observed for the 4.7 nm PbS SCs and 4.6 nm CdSe SCs, respectively. Similarly to our previous study,[18] the films of the NCs showed lower degree of organization and larger average interparticle spacing (Table S2).

Typical load−displacement curves for all of the SCs types and a typical AFM image of the residual indenter impression in CdSe SC are shown in Figure 2. The curves for corresponding

(35) Chudoba, T.; Schwarzer, N.; Richter, F. *Surf. Coat. Technol.* **2000**, *127*, 9–17.
(36) Oliver, W. C.; Pharr, G. M. *J. Mater. Res.* **1992**, *7*, 1564–1583.
(37) Rupich, S. M.; Shevchenko, E. V.; Bodnarchuk, M. I.; Lee, B.; Talapin, D. V. *J. Am. Chem. Soc.* **2010**, *32*, 289–296.

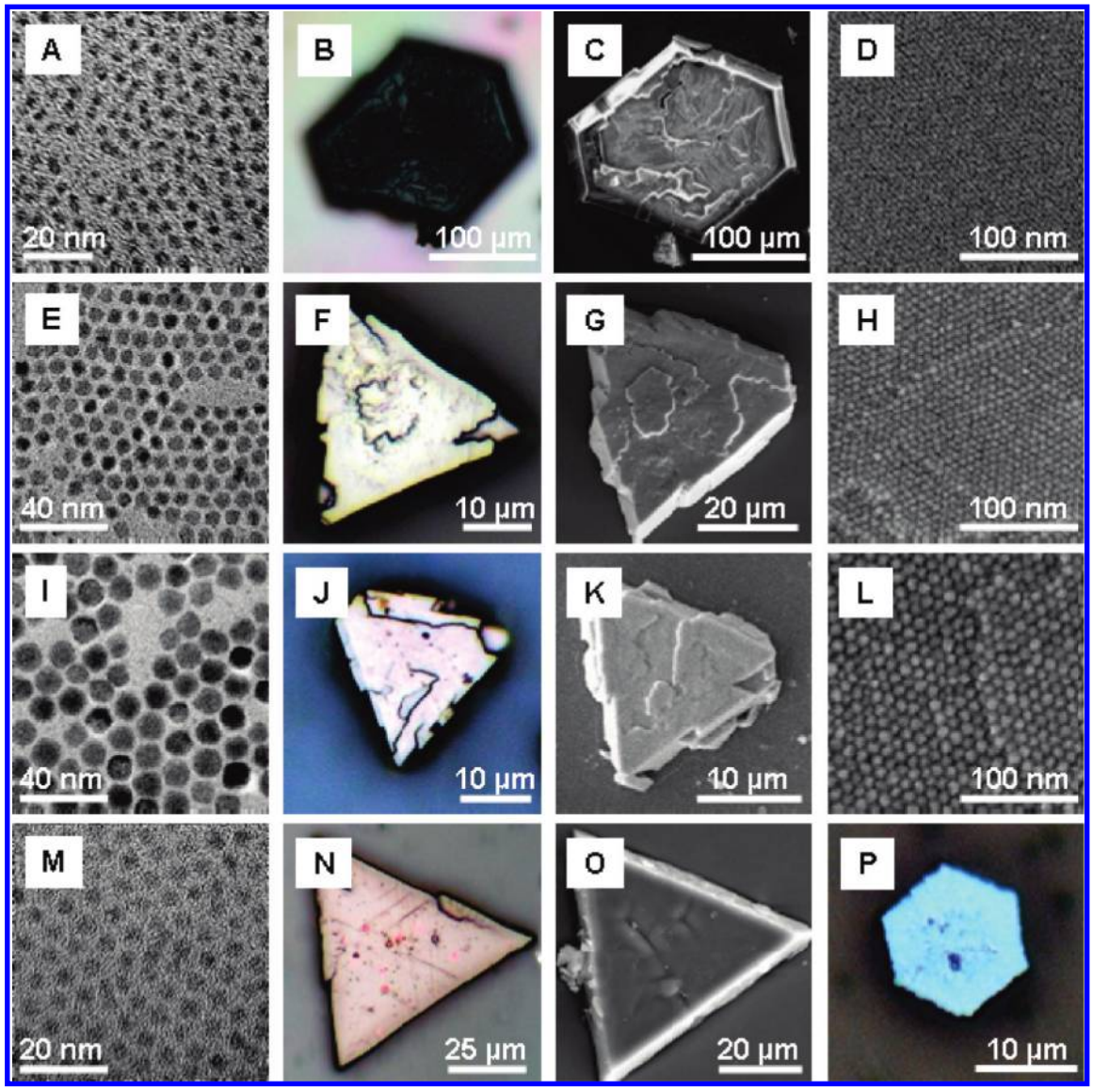

Figure 1. Microscopy images of NCs and their 3D assemblies: (A−D) 4.7 nm PbS NCs; (E−H) 7.1 nm PbS NCs; (I−L) 13 nm PbS NCs; (M−O) 4.6 nm CdSe NCs; and (P) 6.5 nm $CoPt_3$ NCs. The images in panels A, E, I, and M represent HRTEM micrographs of as synthesized NCs. Panels B, F, J, N, and (P) are optical microscopy images collected in reflected light mode. Panels C, G, K, and O are SEM images of the SCs. Panels D, H, and L are HRSEM images of SCs surfaces revealing NCs organization. The images were acquired at the same magnifications.

films are very similar, differing only by the maximum displacement value for the same load. The AFM images showed little or no pileup of displaced material at the edges of the indent, allowing us to use the Oliver-Pharr analysis.[36]

The summary of all of the results is presented in Figure 3 and Table 1. The experiments revealed substantial variation of hardnesses, $H \sim 10-460$ MPa and elastic moduli, $E \sim 0.2-6.1$ GPa (calculated assuming Poisson's ratio, $\nu = 0.33$), across all of the samples. The data represent averages over a penetration depth range up to 20% of samples' thicknesses. The Poisson's ratio used here was suggested by Frenkel and Ladd for hard noninteracting spheres and isotropic materials[38] and it was successfully used previously in the analysis of disordered dense films of CdSe NCs.[27,28] The reduced modulus (E_r, modulus obtained from direct analysis of the load−displacement curves when not accounting for the Poisson's ratio) which is often used for samples with unknown ν, is in the range of ~0.4−13.4 GPa. Furthermore, all of the samples revealed partial elastic recovery as exemplified from the elastic recovery after removal of load (Figure 2B). Since there is obviously viscous behavior as evidenced by the nonrecovered displacement in Figure 2B, the SCs are visco-elastic materials. The overlapping of unloading and loading portions of the curves suggests that volumetric expansion occurs after removal of load (Figure 2B). AFM imaging of a singular residual indent (Figure 2C,D) also revealed slight curvature of the walls, thus, giving further evidence of partial elastic recovery.

Altogether, our data indicate that the SCs have mechanical properties comparable to strong plastics, such as high density polyethylene ($E \sim 1.33$ GPa and $H \sim 20$ MPa) and polymethylmethacrylate ($E \sim 3.75$ GPa).[39] The E for pure macroscopic PbS is ~25−130 GPa depending on crystallographic orientation (bulk modulus, E_{bulk}, a modulus obtained from isotropic

(38) Frenkel, D.; Ladd, A. J. C. *Phys. Rev. Lett.* **1987**, *59*, 1169.

(39) Klapperich, C.; Komvopoulos, K.; Pruitt, L. *Trans. ASME, J. Tribol.* **2001**, *123*, 624–631.

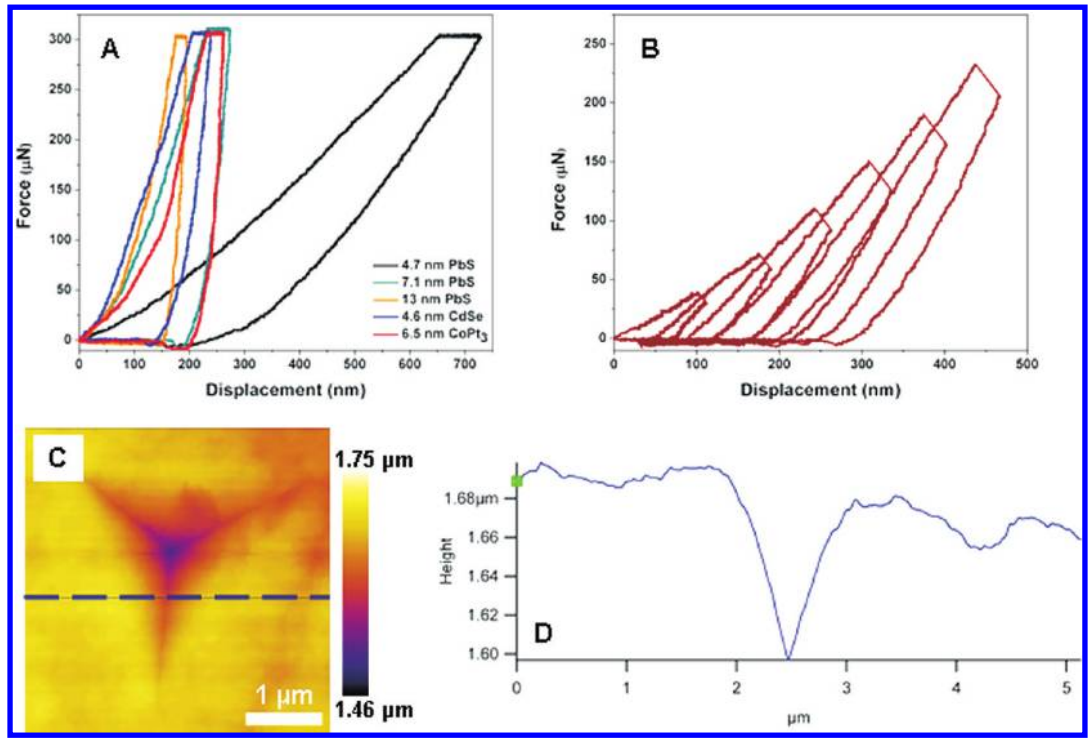

Figure 2. Typical load vs displacement curves for the SCs and AFM image of a residual indent in CdSe SC. (A) Typical load vs displacement curves for the SCs loaded to maximum of 300 μN of force at a constant rate of 50 μN/s. (B) Load−displacement curves for multiple indentations into a single spot showing evidence of elastic recovery. The indents were obtained under displacement control. (C) AFM image of a residual impression of a 300 μN indent in CdSe SC. (D) Cross-sectional profile along the line indicated in panel C showing little or no pileup.

compression as opposed to uniaxial test, is ~62.2 GPa),[40] and Vickers hardness (H_v, hardness obtained from macroscopic indentation measurement) is ~0.59−0.88 GPa.[41] E_{CdSe} is ~13−84 GPa, depending on crystallographic orientation (E_{bulk} ~66 GPa),[42] and E_{CoPt3} is ~100−300 GPa.[43] Our observations are also in a good agreement with theoretical simulations performed on 3D SCs consisting of 1.7 nm Au NCs stabilized with dodecanethiol.[30] The simulation results predicted a modulus of ~1 GPa at room temperature. Conversely, films of electrophoretically deposited 3.2 nm CdSe NCs showed several times larger nanoindentation modulus and hardness (E ~9 GPa and H ~400 MPa) as compared to our data.[28] The difference with our data can be attributed to difference in preparation and postpreparation procedures. Thus cross-linking of capping ligands and thermal treatment were found to increase mechanical properties.[26] As-prepared supraspheres of ~5 nm Au NCs showed E_r and H of a few GPa and a few tens of MPa, respectively.[26] However, the same structures after mild thermal treatment have E_r and H increased to ~10 GPa and ~300 MPa, respectively.

Importantly, all of the 3D assemblies, irrespective of NCs composition, revealed at least 2× greater H and E when compared to the films. These results are opposite to the results recently published by Fava et al. which showed that disordered solids composed of core/shell polymeric spheres had higher stiffness when compared to ordered, fcc-like colloidal crystal from the same spheres.[44] One could argue that the observed differences in our system are related to the presence of a larger amount of free and soft organic ligands in the films. Thermogravimetric (TGA) measurements on PbS NCs revealed 5−15 wt % differences between films and the SCs. (Table S1) However, for CdSe NCs, the ligand amount was found to be nearly identical between the film and SC assembly, and yet there was a 3-fold increase in both H and E in the crystalline structure. The GISAXS experiments showed, in all of the cases, the films had larger interparticle spacing and significantly less organization when compared to the SCs (Table S2). The difference in interparticle spacing and thus in packing density of the NCs may explain the opposite trend observed by Fava et al.[44] In our study, all of the SCs, except for the 4.7 nm PbS NCs, showed strong fcc organization. Theoretical calculations and simulations of hard-sphere colloids predict that the dense fcc structure should be slightly more stable compared to the dense hexagonal close packed (hcp) structure.[45] Interestingly, the smallest PbS NCs showed bcc, while nearly identical in size CdSe NCs showed mixture of fcc and hcp structures. According to TGA data (Table S1), the pairs of 4.7 nm PbS SCs and 7.1 nm PbS films, as well as 7.1 nm PbS SCs and 13 nm PbS films, have almost the same amount of ligands. However, both cases revealed substantial differences in H and slight differences in E. In spite of similar ratio of organic/inorganic components, the SCs from smaller NCs are harder (and slightly stiffer) than films from larger NCs (Figure 3).

Another important result arises from the comparison of PbS samples with different core sizes. We observed a clear trend of

(40) Bhagavantam, S.; Rao, T. S. *Nature* **1951**, *168*, 42–43.
(41) Seltzer, M. S. *J. Appl. Phys.* **1966**, *37*, 4780–4784.
(42) Simmons, G.; Wang, H. *Single-Crystal Elastic Constants and Calculated Aggregate Properties: A Handbook*, 2nd ed.; M.I.T. Press: Cambridge, MA, 1971.
(43) Mehaddene, T.; Kentzinger, E.; Hennion, B.; Tanaka, K.; Numakura, H.; Marty, A.; Parasote, V.; Cadeville, M. C.; Zemirli, M.; Pierron-Bohnes, V. *Phys. Rev. B* **2004**, *69*, 024304.
(44) Fava, D.; Fan, Y. S.; Kumacheva, E.; Winnik, M. A.; Shinozaki, D. M. *Macromolecules* **2006**, *39*, 1665–1669.
(45) Bolhuis, P. G.; Frenkel, D.; Mau, S. C.; Huse, D. A. *Nature* **1997**, *388*, 235–236.

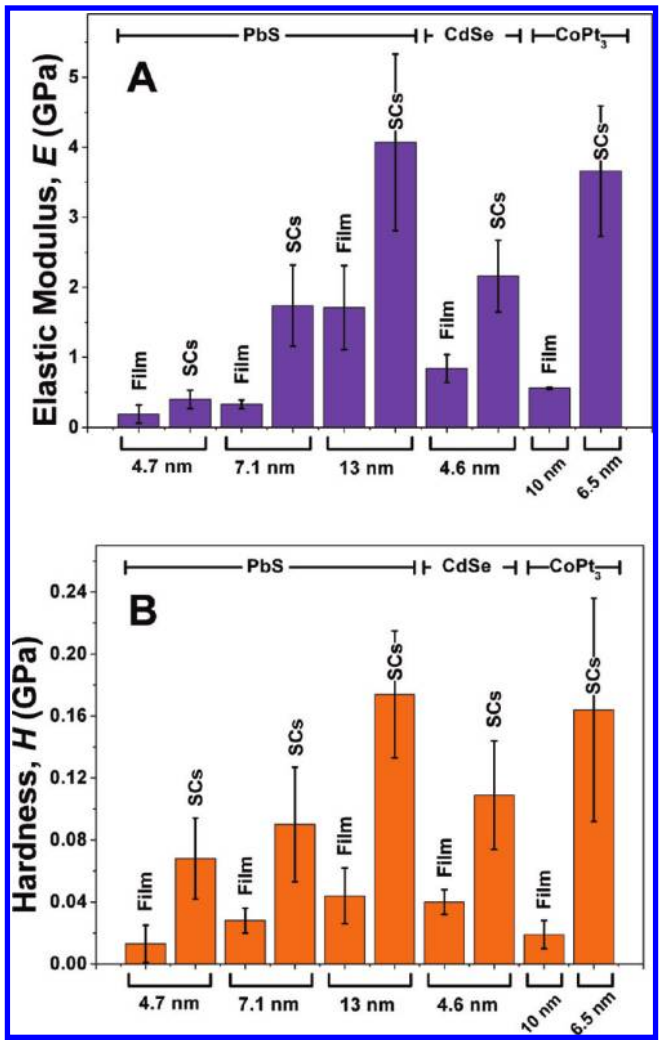

Figure 3. Summary of nanoindentation mechanical results for NCs films with short-ranged order and SCs: (A) elastic moduli and (B) hardnesses. The error bars represent standard deviations of the results for at least 10 indentations.

Table 1. Summary of Nanoindentation Mechanical Properties for Films and SCs Assemblies of Different NCs

sample type	NCs size (nm)	hardness, H (MPa)	reduced modulus, E_r (GPa)	modulus, E (GPa)
PbS^{OA} Film	4.7	13 ± 12	0.42 ± 0.30	0.19 ± 0.13
	7.1	28 ± 8	0.73 ± 0.13	0.33 ± 0.06
	13	44 ± 18	3.80 ± 1.32	1.71 ± 0.60
PbS^{OA} SC	4.7	68 ± 26	0.90 ± 0.30	0.40 ± 0.13
	7.1	90 ± 37	3.87 ± 1.29	1.74 ± 0.58
	13	174 ± 41	8.99 ± 2.78	4.07 ± 1.26
PbS^{PY} SC	4.7	60 ± 19	0.95 ± 0.21	0.43 ± 0.10
	7.1	125 ± 17	6.73 ± 1.84	3.04 ± 0.84
	13	456 ± 87	13.36 ± 2.67	6.06 ± 1.22
PbS^{TOP} SC	7.1	129 ± 49	5.32 ± 1.53	2.40 ± 0.69
CdSe Film	4.6	40 ± 8	1.88 ± 0.43	0.84 ± 0.20
CdSe SC	4.6	109 ± 35	4.78 ± 1.13	2.16 ± 0.51
$CoPt_3$ Film	10	19 ± 9	1.24 ± 0.39	0.56 ± 0.17
$CoPt_3$ Crystal	6.5	164 ± 72	8.09 ± 2.04	3.66 ± 0.93

increasing, both, E and H, with increasing NCs sizes in the films and SCs. Recently, it was shown that during self-assembly process in the case of small NCs ligand−ligand interactions are dominant while interactions of larger NCs are determined by interactions of the hard inorganic cores (van der Waals, electrostatic, dipole−dipole, etc.).[37] GISAXS data show a decrease in the interparticle spacing with an increase of the particle size: 2, 1.9, and 0.9 nm for 4.7, 7.1, and 13 nm large PbS NCs, respectively. We can assume that strong interactions between the inorganic cores are responsible for bringing individual NCs closer to each other as well as for their increasing mechanical properties. While currently there are no literature data on the mechanical properties of NCs superstructures as a function of core sizes, close relatives of the NCs, such as colloidal crystals consisting of large polymer or silica spheres, have been extensively studied.[46−48] A number of studies reported shear moduli (μ) of colloidal crystals, which for an isotropic elastic medium is directly related to the Young's modulus through $E/\mu = 2(1 + \nu)$ (usually both are within the same order of magnitude). Typical values of μ for polymeric colloidal crystals range between 0.01 and 100 Pa and the observed trends show increasing moduli with increasing density or decreasing particle sizes[46] similar to nanocrystalline continuous inorganic materials such as Ag,[49,50] Pb,[49] ZnO,[51] and so forth. *In the SCs, we observe the opposite effect, that is, decreasing stiffness with decreasing NCs sizes*. It is worth mentioning that the same effect was observed in the case of GaAs nanowires.[52] Furthermore, the moduli values for our SCs are at least 6 orders of magnitude greater when compared to the colloidal crystals, even though the largest μ values for colloidal crystals (∼100 Pa) were obtained for polystyrene particles with ∼100 nm sizes, which is only an order of magnitude larger than our largest NCs. Densely packed colloidal crystals from much harder material, SiO_2 spheres (E_{SiO2} ∼70 GPa), also showed dramatically lower E ∼0.3 Pa, for 1.55 μm particles.[48] Natural opals composed of hundreds of nanometer large amorphous SiO_2 spheres ($E_{(bulk\ SiO2)}$ ∼70 GPa) typically display E ∼ 50 GPa and H_v ∼4−6 GPa.[53,54] The spheres in these materials are fused, and hence, they should be treated as porous ceramics rather than ensembles of particles.

The observed behavior in the SCs is more in line with conventional polymeric composites, in which the mechanical properties typically scale up with increasing volume fraction of inorganic material. This suggests that the short organic ligands which are interacting through relatively weak (but numerous) van der Waals forces (and most are liquid at room temperature) form a cohesive organic network surrounding the NCs, reminiscent of a polymer matrix. Using well-known Halpin−Tsai theory developed for polymer nanocomposites and the bulk mechanical properties of the core materials, we can estimate the effective modulus of the OA ligand component.[55] We found that values of E_{OA}, on the order of ∼0.06−0.18 GPa, give nearly perfect fit for all of the different sizes of PbS NCs, both in films

(46) Lindsay, H. M.; Chaikin, P. M. *J. Chem. Phys.* **1982**, *76*, 3774–3781.
(47) Schall, P.; Cohen, I.; Weitz, D. A.; Spaepen, F. *Nature* **2006**, *440*, 319–323.
(48) Schall, P.; Cohen, I.; Weitz, D. A.; Spaepen, F. *Science* **2004**, *305*, 1944–1948.
(49) Cuenot, S.; Fretigny, C.; Demoustier-Champagne, S.; Nysten, B. *Phys. Rev. B* **2004**, *69*, 165410.
(50) Jing, G. Y.; Duan, H. L.; Sun, X. M.; Zhang, Z. S.; Xu, J.; Li, Y. D.; Wang, J. X.; Yu, D. P. *Phys. Rev. B* **2006**, *73*, 235409.
(51) Chen, C. Q.; Shi, Y.; Zhang, Y. S.; Zhu, J.; Yan, Y. J. *Phys. Rev. Lett.* **2006**, *96*, 075505.
(52) Nam, C. Y.; Jaroenapibal, P.; Tham, D.; Luzzi, D. E.; Evoy, S.; Fischer, J. E. *Nano Lett.* **2006**, *6*, 153–158.
(53) Simonton, T. C.; Roy, R.; Komarneni, S.; Breval, E. *J. Mater. Res.* **1986**, *1*, 667–674.
(54) Thomas, P. S.; Smallwood, A. S.; Ray, A. S.; Briscoe, B. J.; Parsonage, D. In *3rd International Indentation Workshop*; Iop Publishing Ltd: Cambridge, England, 2007.
(55) Halpin, J. C.; Kardos, J. L. *Polym. Eng. Sci.* **1976**, *16*, 344–352.

and SCs (see Section 2 in Supporting Information). Observations made for dodecanethiol and TOPO molecules in suspended monolayer of Au NCs[29] and electrophoretically deposited films of 3.2 nm CdSe NCs[27] gave values of E_{thiol} ~4 GPa,[29] and E_{TOPO} ~5.1 GPa,[27] respectively, that reveals a significant difference in mechanical properties between our CdSe SCs and the electrophoretically deposited CdSe NCs.[27,28] In the work of Banerjee et al.,[27] Raman microprobe measurements were used to determine the stress in the crystalline lattice of inorganic CdSe cores, which in turn allowed them to obtain the biaxial modulus for CdSe NPs film and TOPO matrix. In fact, these data were in a good agreement with the data obtained on the same system using nanoindentation.[28] Our measurements with Raman microscopy showed no strain/stress variations across the SCs of 4.6 nm CdSe NCs (Figure S5). Analysis based on Halpin−Tsai model extended to the superlattices of 4.6 nm CdSe and 6.5 nm $CoPt_3$ NCs gives $E_{\text{CdSe-Ligands}}$ ~0.22 GPa for film and ~0.71 GPa for SCs, and $E_{\text{CoPt3-Ligands}}$ ~0.25 GPa for film and ~0.19 GPa for SCs. The difference between our and the other data is most likely not due to the difference in the technique used to measure the mechanical properties, but rather can be attributed to the difference in the preparation of nanocrystal solids. Comparing the systems with two similar sizes stabilized with different ligands (4.6 nm CdSe/TOPO/TOP/HDA and 4.7 nm PbS/OA NCs) revealed substantially greater moduli for CdSe SCs as compared to PbS SCs (Figure 3). According to GISAXS data, SCs of 4.6 nm CdSe and 4.7 nm PbS NCs have fcc and bcc lattices, with space filling factors of 0.74 and 0.68, respectively. This means that up to 26 and 32 vol %, respectively, can remain unoccupied in the SCs of NCs if hard sphere model of packing is assumed. In previous works on Au NCs monolayers[29] or CdSe NCs films,[27,28] the complete filling of voids with free ligands was assumed and structures were considered as homogeneously distributed inorganic NCs in the organic matrix of capping ligands. We cannot exclude the same scenario for SCs. According to GISAXS, SCs of 4.7, 7.1, and 13 nm large PbS NCs have bcc, fcc, and fcc lattices, respectively (Figure S4 and Table S2). Simple geometrical calculations give us 28, 12.7, and 7.1 wt % of the oleic acid content in SCs if we assume complete filling of the unit cell space not occupied by inorganic cores and density of oleic acid and PbS equal to 0.895 (liquid state) and 7.6 g/cm^3, respectively. These numbers are in relatively good agreement with the TGA data that revealed 28, 12.5−15, and 9 wt.% of oleic acid for SCs consisted of 4.7, 7.1, and 13 nm PbS NCs, meaning that indeed there is no unoccupied voids in the SCs. This evidence further differentiates our system from colloidal crystals reported in Fava's work,[44] where jamming of shearing along crystallographic planes during deformation was directly observed in stress−strain and nanoindentation curves, and was suggested as a mechanism for reinforcement in disordered samples. Our nanoindentation curves (Figure 2A,B) show completely smooth development irrespective of the sample type, suggesting continuity of the solid matrix due to filling of the empty voids with ligands.

For the 4.7 nm PbS NCs, the GISAXS experiments showed center-to-center distance of only ~6.6 nm in the SCs. This leaves an average of ~1.9 nm of interparticle spacing. The length of OA is 1.8 nm. Conversely, the CdSe NCs are stabilized primarily with TOPO and TOP (with a small presence of HDA),[56] which have saturated but much shorter, 8-carbon long chains. The length of TOPO molecule from geometrical considerations is ~1.1 nm. In the case of CdSe SCs, the GISAXS revealed center-to-center distance of ~6.1 nm, which gives interparticle spacing of ~1.5 nm. The explanation for the enhancement of mechanical properties in 4.6 nm CdSe SCs as compared with the 4.7 nm PbS SCs can be associated with the difference in the ligands passivating the surface of NCs. The role of ligands has been emphasized for Au NCs 2D lattice and binary superlattices.[29,57] The OA molecules coating the PbS NCs contain a double bond in the middle of the hydrocarbon chain between the 9th and 10th carbon atoms (Figure S1). This can impart a bent conformation to the molecule which can potentially hinder interdigitation of the ligands between adjacent NCs. In reality, the structural organization of ligands inside SCs is not known and should be further investigated through a combination of experimental and simulation efforts. Also we cannot ignore the fact that the 4.6 nm CdSe are more tightly packed due to the fcc type of the SC's lattice when compared to the bcc lattice self-assembled by 4.7 nm PbS NCs. In principle, less packed organization of individual NCs can be responsible for smaller E and H. However, 7.1 nm PbS NCs form fcc-type of SCs with E and H similar to those of fcc-like SCs consisting of 4.6 nm CdSe, meaning that packing arguments only cannot explain the enhanced mechanical properties of 4.6 nm CdSe SCs as compared with 4.7 nm PbS SCs.

To further explore the effect of ligand chemistry on the mechanical properties of the SCs, we have investigated ligand exchange and ligand-directed structuring of the SCs (Figure 4 and Table 1). The choice of ligands was justified by considering the following arguments. First of all, we observed better mechanical properties for SCs of CdSe NCs stabilized by the mixture of TOPO/TOP/HDA with the molar ratio 5:1:0.8 as determined by XPS.[56] Also it has been shown that molecules of TOP can bind to the S sites at the surface of PbS NCs.[58] Pyridine was chosen as an agent affecting the solubility of nanocrystals in polar solvents[59] that can result in slower destabilization of colloidal solution. We introduced ~6-fold excess of new ligands into the solutions of 7.1 nm PbS NCs during the growth of SCs. We found that both pyridine and TOP increased E and H by ~50% (Figure 4 and Table 1). The GISAXS experiments showed almost the same center-to-center spacing when pyridine was added (~8.9 nm) as when the SCs were grown with native OA ligands. Additions of TOP resulted even in some increase of center-to-center spacing up to 9.3 nm. However, in both cases, preferential (111) orientation of SCs parallel to the substrate was observed meaning that most of the SCs were parallel to the substrate. Taking into account that mechanical properties depend on the crystallographic orientation in the case of atomic crystals, we can assume that higher values of H and E are associated with preferential orientation of supercrystals grown in the presence of TOP and pyridine. Also, we speculate that the addition of TOP to the assembly passivates the surface S sites[58] and increases the stability of NCs against aggregation leading to the slower destabilization of colloidal solution. It can similarly improve the connectivity between the NCs in the SCs by increasing the number of interacting hydrocarbon chains. The addition of pyridine led to increase of

(56) Borchert, H.; Talapin, D. V.; McGinley, C.; Adam, S.; Lobo, A.; de Castro, A. R. B.; Moller, T.; Weller, H. *J. Chem. Phys.* **2003**, *119*, 1800–1807.
(57) Chen, Z. Y.; Moore, J.; Radtke, G.; Sirringhaus, H.; O'Brien, S. *J. Am. Chem. Soc.* **2007**, *129*, 15702–15709.
(58) Lobo, A.; Moller, T.; Nagel, M.; Borchert, H.; Hickey, S. G.; Weller, H. *J. Phys. Chem. B* **2005**, *109*, 17422–17428.
(59) Murray, C. B.; Norris, D. J.; Bawendi, M. G. *J. Am. Chem. Soc.* **1993**, *115*, 8706–8715.

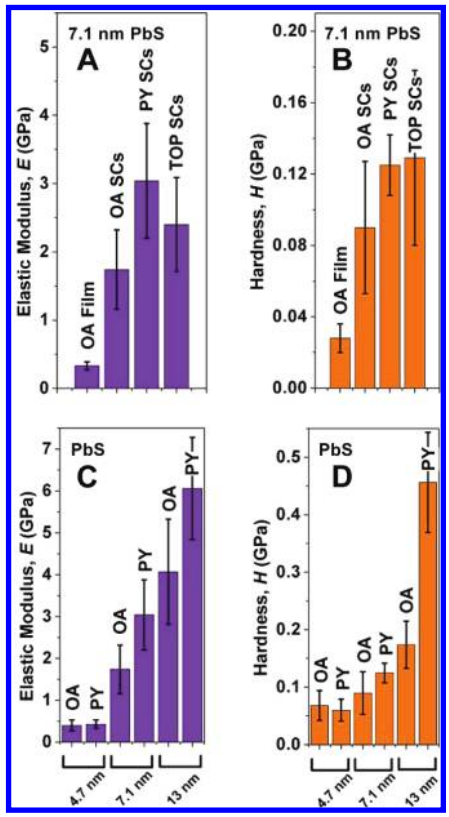

Figure 4. Summary of ligand addition effect on mechanical properties. (A and B) Comparison of elastic moduli and hardnesses for 7.1 nm PbS NCs with different ligands, and (C and D) comparison of elastic moduli and hardnesses for different sizes of PbS with addition of pyridine. The error bars represent standard deviations of the results for at least 10 indentations.

mechanical properties (to a different degree) for SCs assembled from larger, 13 nm PbS NCs. On the other hand, note that the addition of pyridine to 4.7 nm PbS NCs resulted in the formation of fcc-type SCs while it did not significantly affect the mechanical properties. Interparticle spacing in fcc-like SCs of 4.7 nm PbS NCs was smaller as compared with bcc-like SCs (Table S2). This can indicate that in SCs assembled from small NCs with high surface to volume ratio, and as a result with high concentration of ligands in superstructure, the role of organic ligands is dominant in determining the mechanical properties. Interpretation of FTIR scans does not allow us to make conclusions about incorporation of pyridine molecules into the SCs, while XPS revealed a trace amount of N atoms in the 4.7 nm PbS SCs but not in the 7.1 nm PbS SCs. (Figures S6−S8). Thus, it appears that pyridine does in fact slow down destabilization of the colloidal solutions and subsequently affects crystallization of the SCs. The XPS experiments have shown a small presence of P atoms (Figure S9), which can only originate from the TOP molecules. Similarly, TGA showed ∼4 wt % increase in the amount of organic component in the TOP-PbS SCs (Table S1).

Conclusions

Systematic study of collective mechanical response of 3D NC solids demonstrated that the hardness and stiffness of SCs falls in between the hard sphere colloidal crystals and opals. The SCs have more similarities with strong plastics, although with greater hardness. The collective behavior of the surface ligands, exhibiting polymer-like stiffness and elasticity, is also unusual and unique. The experiments on the films self-assembled from different types of NCs revealed elastic moduli E in the range of ∼0.2−1.7 GPa and hardnesses, H, in the range of ∼10−40 MPa. The corresponding properties for the SCs were E ∼0.4−6 GPa and H ∼40−450 MPa. In all of the sample types, the SCs revealed at least 2-fold greater H and E (as high as 10-fold for H) when compared to the films. Comparison of mechanical properties for a series of different NCs sizes, that is, 4.7, 7.1, and 13 nm PbS NCs, revealed a direct relationship between the size of the inorganic core and the mechanical properties of the ensemble, yielding increasing H and E with increasing core size. These results further reinforce the plastic-like behavior of the SCs, and make the SCs comparable to nanoparticle-filled polymers, that is, nanocomposites. With proper design of the ligand's chemistry, the properties of the SCs could be further tuned and explored for variety of advanced devices.

Acknowledgment. Work at the Center for Nanoscale Materials and Molecular Foundry were supported by the Office of Science, Office of Basic Energy Sciences, of the U.S. Department of Energy under Contract Nos. DE-AC02-06CH11357 and DE-AC02-05CH11231, respectively. P.P. thanks the support of Willard Frank Libby postdoctoral fellowship from Argonne National Laboratory.

Supporting Information Available: TGA analysis, FTIR spectra, summary of GISAXS scans, summary of Raman microscopy imaging, details of ligands' mechanical properties calculations, and XPS scans. This material is available free of charge via the Internet at http://pubs.acs.org.

JA100464A